Available online at www.sciencedirect.com
ScienceDirect
Journal of Photochemistry and Photobiology A: Chemistry 189 (2007) 301–306
Journal of Photochemistry and Photobiology A:Chemistry
www.elsevier.com/locate/jphotochem

Dye-sensitized solar cells with Pt–NiO and Pt–TiO_2 biphase counter electrodes

Seok-Soon Kim [a], Kyung-Won Park [b], Jun-Ho Yum [a], Yung-Eun Sung [c,*]

[a] *Department of Materials Science and Engineering, Gwangju Institute of Science and Technology (GIST), Gwangju 500-712, South Korea*
[b] *Department of Chemical and Environmental Engineering, Soongsil University, Seoul 156-743, South Korea*
[c] *School of Chemical and Biological Engineering, Seoul National University, Seoul 151-744, South Korea*

Received 19 September 2006; received in revised form 28 December 2006; accepted 20 February 2007
Available online 23 February 2007

Abstract

New type counter electrodes comprised of Pt and a metal oxide biphase, Pt–NiO and Pt–TiO_2, were prepared by RF magnetron co-sputtering system for use in dye-sensitized solar cells. Transmission electron microscope images confirmed the formation of ~3 nm nanosized Pt polycrystalline mixed with metal oxide phase, which has higher active surface area than a conventional Pt electrode. When the Pt–TiO_2 counter electrode was used in the cell, the power conversion efficiency was increased up to ~1.56 times, compared to conventional devices composed of a Pt electrode under 1 Sun with air mass 1.5 Global illumination due to its superior electrocatalytic activity and efficient reflection of incident light at the counter electrode.

Keywords: Dye-sensitized solar cell; Counter electrode; Sputtering system; Pt–NiO; Pt–TiO_2

1. Introduction

The dye-sensitized solar cell (DSSC) comprised of a dye-modified wide band semiconductor electrode, a counter electrode, and an electrolyte containing a redox couple (I^-/I_3^-) is an alternative to conventional silicon or compound semiconductor solar cells due to its low fabrication cost, permanence, environmental compatibility, and simple fabrication process [1,2]. The photoexcitation of dye molecules under illumination leads to the injection of an electron from the excited state of the dye to the conduction band of the semiconductor, which flows through the external circuit. Simultaneously, the oxidized dye is reduced by a redox mediator in the electrolyte and returns to the ground state. The electrons that flow through the external circuit arrive at the counter electrode and participate in the regeneration of triiodide, according to reaction $I_3^- + 2e^- = 3I^-$ [3–5].

In spite of the cost-efficiency of DSSC, for practical applications, many groups have attempted to improve efficiency and long-term stability focusing on some aspectsm, such as minimization of recombination at the electrode and electrolyte interface using coupled semiconductor systems and passivation of the semiconductor surface [6–11], the development of new dye molecules which absorb all the visible and near infra red light [12–14], and the fabrication of a solid-state DSSC by replacing the liquid electrolyte [15–19], etc., whereas, only a few studies of the counter electrodes in DSSC have been reported [20–28]. The best candidate for use as a counter electrode is Pt metal due to its superior electrocatalytic activity. Papageorgiou et al. prepared nanosized Pt metal clusters by the thermal decomposition of H_2PtCl_6 from isopropanol on a transparent conducting oxide (TCO) coated substrate to maximize the catalytic activity of Pt on the reduction of iodine or triiodide [20]. Hauch and Georg prepared several Pt electrodes by various methods including electron beam evaporation, sputtering, and the thermal decomposition of H_2PtCl_6 and characterized the electrolyte/Pt interface by electrochemical impedance spectroscopy [21]. They concluded that the sputtered Pt electrode was superior to the others due to its low charge transfer resistance, moderate porosity that provides a high effective surface area, and good adhesion of the Pt layer onto the transparent conducting oxide (TCO) substrate.

In addition, Saito et al. and Suzuki et al. reported the use of a chemically produced conducting polymer and carbon nanotubes in the counter electrode, respectively [22–24]. In these

* Corresponding author. Tel.: +82 2 880 1889; fax: +82 2 888 1604.
E-mail address: ysung@snu.ac.kr (Y.-E. Sung).

1010-6030/$ – see front matter © 2007 Elsevier B.V. All rights reserved.
doi:10.1016/j.jphotochem.2007.02.019

cases, although the cost of fabrication can be decreased, the conversion efficiency is relatively low compared to a cell with a Pt counter electrode. Based on these reports, we demonstrated the preparation of a new type of counter electrode consisting of a Pt nanosized phase in a porous NiO phase using a co-sputtering system [25]. This procedure not only improved the electocatalytic activity of counter electrode by increasing the active surface area and adhesion, but also permitted the manufacturing cost to be reduced.

In this paper, we report on the characterization of DSSCs with a new type counter electrodes comprised of Pt and a metal oxide biphase, Pt–NiO and Pt–TiO_2, prepared by RF magnetron co-sputtering system.

2. Experimental

Two types of biphase counter electrodes, Pt–NiO and Pt–TiO_2, were prepared by means of an RF magnetron co-sputtering system on Fluorine-doped SnO_2-layered glass substrates (FTO glass substrate, Asahi glass Co., Ltd., sheet resistance: 10 Ω/□). Elemental Pt, NiO, and TiO_2 were used as the target materials. The base pressure was less than 5×10^{-6} Torr and the working pressure was 5×10^{-3} Torr for all electrodes. The sputtering was performed under an atmosphere of Ar at 40 sccm at room temperature. The power of the Pt, NiO, and TiO_2 sputtering guns was individually manipulated to fabricate Pt–NiO and Pt–TiO_2 electrodes which have similar Pt crystalline sizes and surface areas. For comparison, a Pt electrode was also grown with the same thickness with biphase electrodes, Pt–NiO and Pt–TiO_2. To confirm the formation of nanosized Pt polycrystalline phase mixed with the metal oxide phase, high resolution transmission electron microscopy (HRTEM, Phillips CM20T/STEM Electron Microscope at an accelerating voltage of 200 kV) images were obtained. For the preparation of a sample for use in an HRTEM measurement, a Cu grid was used as the substrate during the growth process. The light reflecting properties of various counter electrodes, a Pt electrode and two types of biphase electrodes, Pt–NiO and Pt–TiO_2, were compared by measuring the UV–vis reflection spectra.

The active surface area and electrocatalytic activity of three types of counter electrodes, Pt, Pt–NiO, and Pt–TiO_2, was verified by measuring cyclic voltammograms (CVs). By comparing the charge corresponding to the hydrogen adsorption/desorption on the three types of electrodes in a cyclic voltammogram of aqueous solutions containing 0.1 M NaOH at room temperature saturated with nitrogen using a conventional three electrode system, active surface area was verified.

The cyclic voltammetry of I^-/I_3^- redox mediator on three types of counter electrodes was carried out in an acetonitrile solution of 10 mM LiI, 1 mM I_2 and 0.1 M $LiClO_4$ with three electrode systems to compare the electrocatalytic activity of electrodes on the regeneration of redox mediator.

To compare the performance of the Pt single phase and two types of biphase electrode, Pt–NiO and Pt–TiO_2, as a counter electrode, solar cells were fabricated by a conventional method. Commercial TiO_2 paste (Ti-Nanoxide T, Solaronix Co., Ltd.) was cast on the FTO glass substrates with a doctor-blade and then sintered at 450 °C for 30 min. These TiO_2 coated films were immersed in a solution of Ru 535 dye (Solaronix Co., Ltd.) for a day. The dye-modified TiO_2 electrode and various counter electrodes, Pt, Pt–NiO, and Pt–TiO_2, were sandwiched and the inner space was filled with a liquid electrolyte containing 0.5 M LiI and 0.05 M I_2 as a redox mediator. Cell performance was measured under 1 sun using a xenon light source and an air mass 1.5 global filter. Photocurrent–voltage (*I–V*) measurements were performed using an Autolab PGSTAT30 Potentiostat/Galvanostat. Here, the area of the fabricated cells was constant at 0.5 cm × 0.5 cm.

3. Results and discussion

When the Pt was sputtered, the atoms that arrived at the substrate diffuse and form islands due to preferentially strong binding to each other than to the substrate. The coalescence of islands then leads to the formation of smooth films as shown in Fig. 1(a). In contrast, when the Pt was simultaneously sputtered with the metal oxide, thermodynamically stable phase separation occurred between Pt and the metal oxide and the coalescence of Pt islands was limited due to the presence of metal oxide, thus leading to the formation of new types of electrodes composed of a Pt nanocrystalline phase mixed with a metal oxide phase, as shown in Fig. 1(b) [29]. In this new electrode system, the increase of the active surface area of the Pt compared to that of a single Pt film electrode would be expected. The formation of a Pt nanocrystalline phase mixed with metal oxide was confirmed from the TEM images.

Fig. 2 shows HRTEM images of Pt, Pt–NiO, and Pt–TiO_2 deposited on a Cu grid under the same conditions which were used in the preparation of Pt and Pt–metal oxide on the FTO glass substrate. In contrast to Fig. 2(a), which shows an image of a Pt film deposited on a Cu grid, Fig. 2(b and c) shows the successful formation of a Pt nanocrystalline phase mixed with NiO and TiO_2, respectively, as the result of the thermodynamically stable phase separation between Pt and the metal oxide and also limitations in the extent of coalescence of Pt islands due to the presence of the metal oxide. Here, the size of Pt crystals in the NiO and TiO_2 matrix was found to be ∼3 nm as shown in Fig. 2(b and c). In addition, the lattice spacings of the Pt (1 1 1) and (2 0 0) planes were observed to be 0.227 nm and 0.196 nm, respectively (see the (1 1 1) spacing in the inset of Fig. 2(d)). The formation of Pt nanostructures with crystallinity was also confirmed by the diffraction patterns and these data are shown in the inset of Fig. 2(d). In contrast to the appearance of clear spot in the TED patterns of only Pt part, in the TED pattern of NiO, a cloudy area was observed. This indicates the formation of amorphous NiO (not shown here). The formation of polycrystalline Pt mixed with amorphous NiO was also confirmed by the XRD patterns of Pt and Pt–NiO electrode. The (1 1 1) peak at 39.8° was dominant and (2 0 0) peak was also present at 46.2° (see the (2 0 0) peak in the inset of Fig. 2(e)). This indicates that polycrystalline Pt was formed. In addition, the absence of a peak corresponding to NiO at 43.2° indicates the formation of polycrystalline Pt mixed with amorphous NiO. Generally, when the oxide is prepared by sputtering at room temperature,

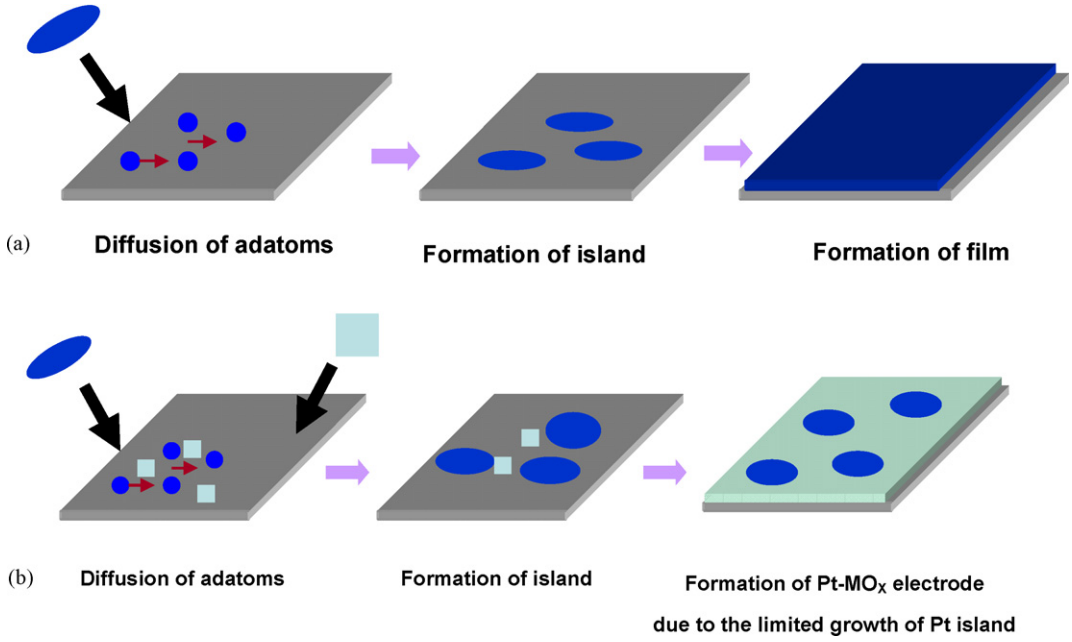

Fig. 1. Schematic growth process of (a) Pt electrode and (b) Pt and metal oxide biphase electrode using a co-sputtering system.

it has amorphous property, in contrast to the formation of polycrystalline Pt by sputtering at room temperature. In the Pt–TiO_2 electrode, same structural properties are observed. As can be seen in Fig. 2, we prepared the Pt–NiO and Pt–TiO_2 electrodes which have the same sized Pt nanocrystalline phase. The aim of this study is to demonstrate the effect of the reflectance of the counter electrode on the device performance of DSSCs using high refractive index TiO_2 instead of NiO, because one of the most important requirements for a counter electrode in DSSC is light-reflecting ability to improve light-harvesting efficiency. Based on the following equation, the increase of reflectance with higher refractive index can be expected and we measured the reflectance of thee types of electrodes with the perfect mirror reference under the assumption of no absorption or scattering (based on the R (reflectivity) + T (transmissivity) = 1).

$$R = \frac{(n-1)^2 + k^2}{(n+1)^2 + k^2} \quad (1)$$

where n is the refractive index and k is thedamping constant, for dielectrics 10^{-7}.

The light-reflecting property of various counter electrodes, Pt, Pt–NiO, and Pt–TiO_2, was compared by measuring UV–vis reflection spectra. Here, we prepared thin Pt or Pt and metal oxide biphase electrodes which are relatively transparent and do not have a mirror-like surface property, in order to more accurately investigate the effect of the reflectance of the counter electrode on device performance. As shown in Fig. 3, the reflectance of Pt–TiO_2 was increased about 1.5 times compared to the single Pt or Pt–NiO biphase electrode at the wavelength region corresponding to the absorption maximum of Ru 535 dye molecules which is used as the sensitizer in the fabrication of DSSCs. We conclude that the increase in the reflectance of the Pt–TiO_2 electrode is due to the high refractive index value for TiO_2.

When the incident light arrives at the photoelectrode through the transparent electrodes, the light induces the excitation of the sensitizer, Ru 535 dye molecules, and pass through the counter electrode (the process 1 in Fig. 4) or are reflected at the counter electrode (the process 2 in Fig. 4). In the latter case, efficient excitation of dye molecules can be expected, as shown the schematic representation in Fig. 4. Here, the application of a high reflectance Pt–TiO_2 electrode as the counter electrode in DSSCs, can result in the improvement in the photocurrent as the result of the efficient excitation of dye molecules by the increased 2 process in Fig. 4.

Before applying various counter electrodes to the fabrication of DSSCs, the active surface area of Pt was verified by comparing the charge corresponding to hydrogen adsorption/desorption on a Pt electrode, a Pt–NiO, and Pt–TiO_2 biphase electrode in a cyclic voltammogram of aqueous solutions (not shown here). The surface area of Pt–NiO and Pt–TiO_2 biphase electrodes are two times that of the Pt electrode with the same thickness. From this result, increased electrocatalytic activity and reduced manufacturing cost can be expected by using Pt–metal oxide biphase electrode as a counter electrode in DSSCs.

The CVs of I^-/I_3^- redox mediator on the three types of counter electrodes are shown in Fig. 5. As shown in Fig. 5, the oxidation and reduction peaks of I^-/I_3^- on the three types of electrodes were similar and an increased current density was observed when the Pt–NiO and Pt–TiO_2 electrode was used as the working electrode. The higher current density means superior electrocatalytic activity of Pt–metal oxide biphase electrodes to the conventional Pt electrode, which is attributed to the increase of active surface area due to the formation of nanosized Pt crystalline by co-sputtering systems. In addition, similar electrocatalytic activity of Pt–NiO and Pt–TiO_2 electrode on the regeneration of redox mediator can be expected from the similar current density in Fig. 5. Here, the electrical

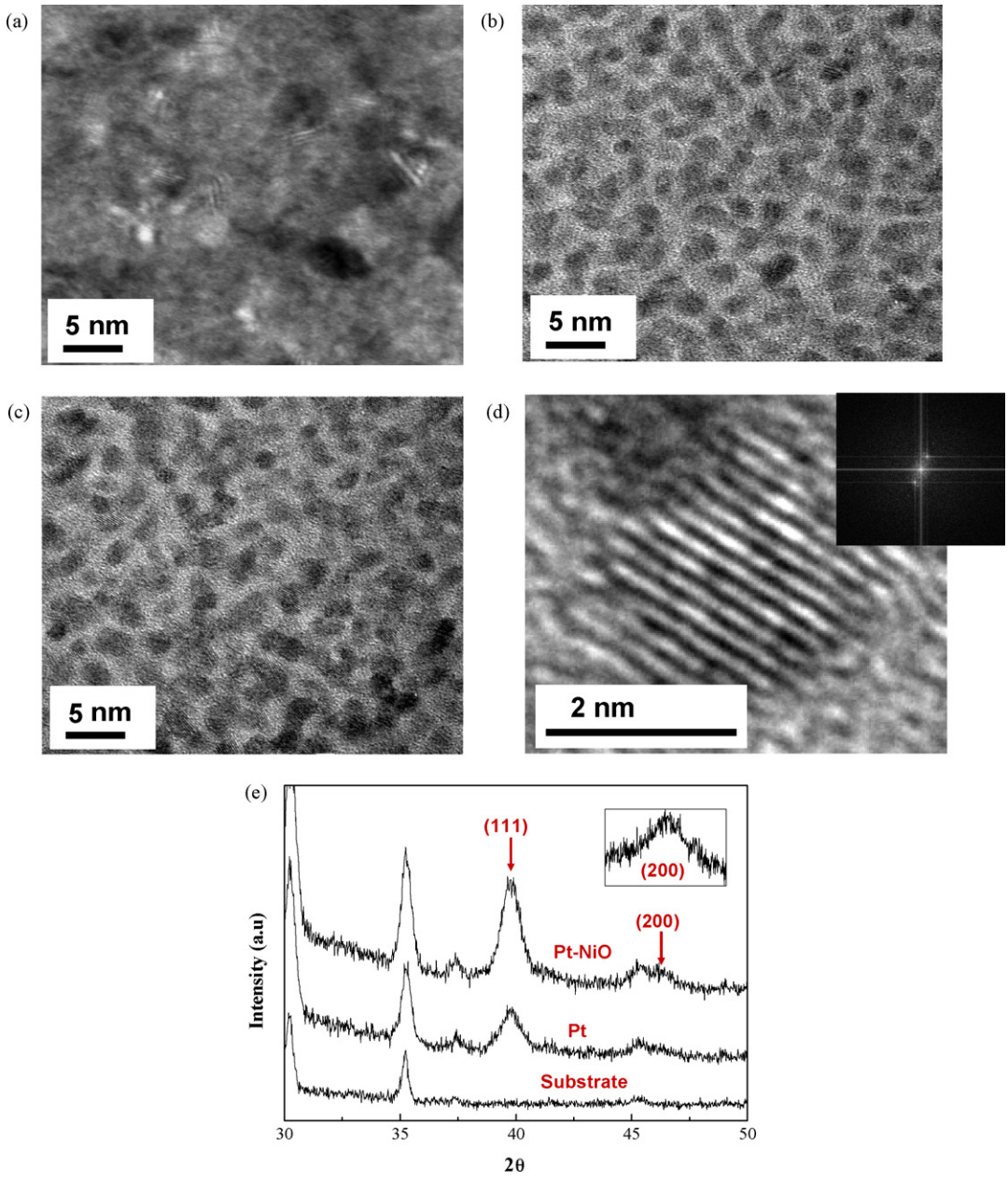

Fig. 2. Transmission electron microscope (TEM) image of (a) Pt, (b) Pt–NiO, and (c) Pt–TiO_2 electrode prepared using a co-sputtering system. (d) High resolution transmission electron microscope (HRTEM) image of Pt nanophase in TiO_2 matrix, showing the (1 1 1) spacing of Pt and Transmission electron diffraction (TED) patterns. (e) X-ray diffraction (XRD) patterns of Pt, Pt–NiO and Pt–TiO_2 electrodes.

connectivity between Pt is one of the most important factors to determine the charge transfer resistance at the counter electrode. One of the advantages of co-sputtering method to fabricate nanophase Pt mixed with oxide is tunable size and density of Pt nanophase. The electrical connectivity and electrocatalytic activity of biphase electrode are strongly dependent on the density of Pt nanophase, which can be changed by controlling the RF power during co-sputtering process. If the RF power on the oxide target is increased, relatively low density of Pt may be observed due to the relatively fast deposition rate of oxide. Based on this point, we optimized the conditions for the fabrication of excellent Pt-oxide counter electrode, which has higher active surface area without increase in the charge transfer resistance resulting from the poor electrical connectivity between Pt nanophases. As shown in Fig. 2(b and c), the density of Pt is sufficiently high and the Pt nanophases are connected each other. Hence, improved electrocatalytic activity of biphase electrode, resulting from the higher active surface area without increase of charge transfer resistance at the counter electrode, can be obtained as shown in Fig. 5. In addition, similar charge transfer resistance was observed in the measurements of ac impedance spectra with the sandwich type electrochemical cells consisting of two identical counter electrodes (not shown here).

Based on these results, three types of DSSC were fabricated using Pt, Pt–NiO, and Pt–TiO_2 as counter electrodes and their performances were compared. Fig. 6 shows the resulting

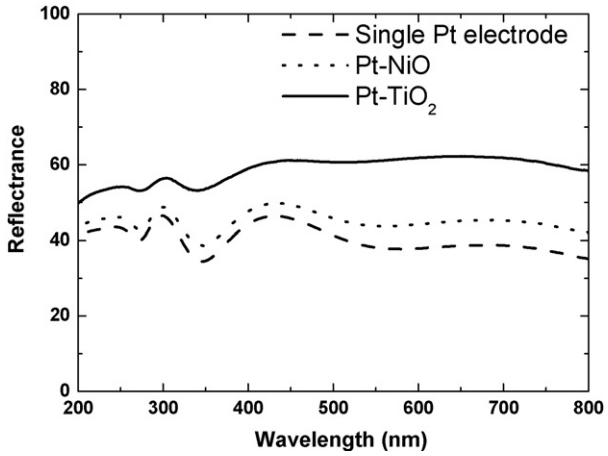

Fig. 3. UV–vis reflection spectra of the three types of electrodes, Pt, Pt–NiO, and Pt–TiO_2.

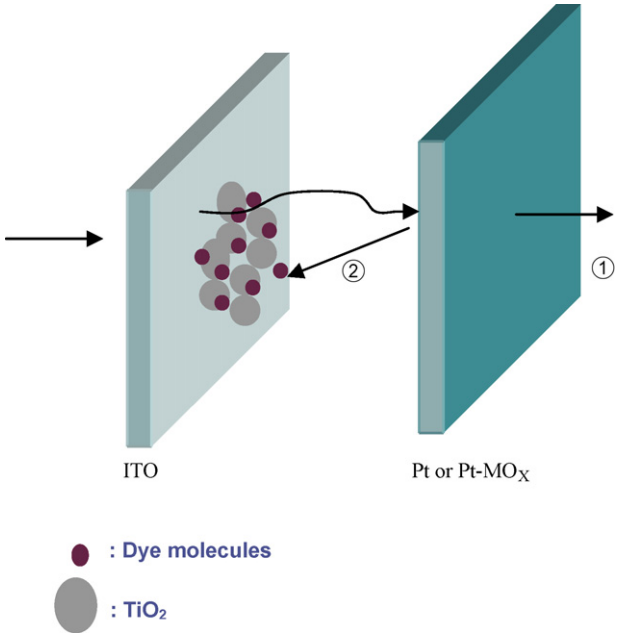

Fig. 4. Expected process at the counter electrode after the excitation of dye molecules by incident light. (1) Transmit through the counter electrode and (2) Reflect at counter electrode and lead to the excitation of dye molecules.

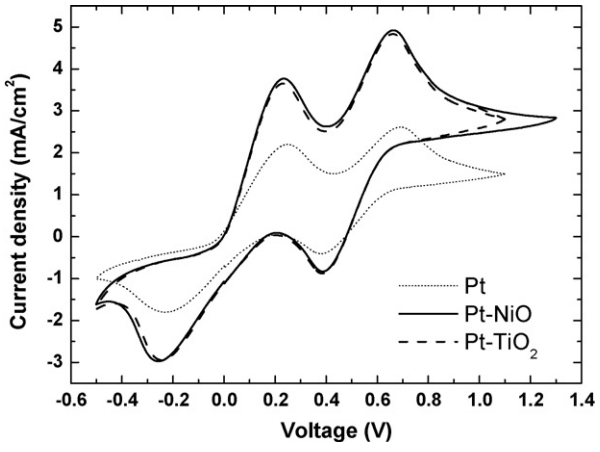

Fig. 5. Cyclic voltammograms of the electrodes in acetonitrile solution of 10 mM LiI, 1 mM I_2 and 0.1 M $LiClO_4$.

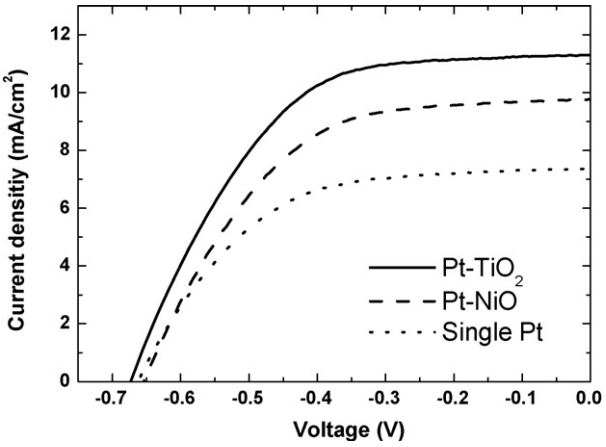

Fig. 6. *I–V* curves for conventional liquid-state DSSCs fabricated using Pt, Pt–NiO and Pt–TiO_2 counter electrodes.

photocurrent–voltage curves for conventional DSSCs fabricated with a liquid electrolyte using three types of counter electrodes, Pt, Pt–NiO, and Pt–TiO_2 electrode. When the Pt–metal oxide biphase electrode was used, the short-circuit current density and cell efficiency were increased as the result of the increased active surface of the nanosized Pt in the Pt–metal oxide biphase electrode. Specially, when the Pt–TiO_2, which has a high reflectance compared to the Pt and Pt–NiO electrode and similar active surface area with the Pt–NiO electrode, was used as the counter electrode, the efficiency was increased up to 56% compared to the cell with a conventional Pt counter electrode due, not only to increased active surface area but also to efficient reflection of incident light at the counter electrode results in a high light-harvesting efficiency. The overall conversion efficiency was increased from 2.70 to 3.62 and 4.21% via the use of Pt–NiO and Pt–TiO_2 biphase electrodes, respectively.

In contrast to the increase in short-circuit current as the result of using the Pt–NiO and Pt–TiO_2 biphase electrode, the open-circuit voltage remained unchanged. Because the open-circuit is considered as the difference between the fermi level of the semiconductor and the redox potential of the redox couple, constant open-circuit voltage can be explained indirectly from the similar CVs for I^-/I_3^- (shown in Fig. 5).

4. Conclusions

Two types of new counter electrodes, composed of a nanosized Pt polycrystalline phase mixed with NiO or TiO_2, for DSSC were fabricated by means of a co-sputtering system to improve cell performance and reduce manufacturing costs. The formation of a ~3 nm nanosized Pt polycrystalline phase mixed with NiO or TiO_2 was confirmed by HRTEM images and TED patterns. By applying Pt and a metal oxide biphase electrode, the short-circuit current density and cell efficiency were increased as the result of the increased active surface of the nanosized Pt in the Pt and metal oxide biphase electrode. Specially, when Pt–TiO_2, which has high reflectance compared to Pt and Pt–NiO electrodes, was used as the counter electrode, the efficiency was increased up to 56% compared to a cell with a conventional Pt

counter electrode. This was due to, not only an increase in active area but also the efficient reflection of incident light at the counter electrode, which result in a high light-harvesting efficiency. The overall conversion efficiency was increased from 2.70 to 3.62 and 4.21% by applying Pt–NiO and Pt–TiO_2 biphase electrode, respectively, under 1 sun with an air mass 1.5 Global filter.

Acknowledgements

This work was supported by KOSEF (Grant No. R01-2004-000-10143) and the Research Center for Energy Conversion and Storage. SSK acknowledges support by the Brain Korea 21 project from the Ministry of Education.

References

[1] B. O'Regan, M. Grätzel, Nature 353 (1991) 737.
[2] L.M. Peter, K.G.U. Wijayantha, Electrochim. Acta 45 (2000) 4543.
[3] K. Kalyanasundaram, M. Grätzel, Coord. Chem. Rev. 77 (1998) 347.
[4] Y. Shen, H. Deng, J. Fang, Z. Lu, Colloids Surf. A: Physicochem. Eng. Aspects 175 (2000) 135.
[5] G. Smestad, C. Bignozzi, R. Argazzi, Sol. Energy Mater. Sol. Cells 32 (1994) 259.
[6] W.-P. Tai, Sol. Energy Mater. Sol. Cells 76 (2003) 65.
[7] P.K.M. Bandaranayake, P.V.V. Jayaweera, K. Tennakone, Sol. Energy Mater. Sol. Cells 76 (2003) 57.
[8] B.A. Gregg, F. Pichot, S. Ferrere, C.L. Fields, J. Phys. Chem. B 105 (2001) 1422.
[9] C. Nasr, P.V. Kamat, S. Hotchandani, J. Electroanal. Chem. 420 (1997) 201.
[10] S.-S. Kim, J.-H. Yum, Y.-E. Sung, Sol. Energy Mater. Sol. Cells 79 (2003) 495.
[11] S.-S. Kim, J.-H. Yum, Y.-E. Sung, J. Photochem. Photobiol. A: Chem 171 (2005) 269.
[12] T. Ma, K. Inoue, H. Noma, K. Yao, E. Abe, J. Photochem. Photobiol. A: Chem. 152 (2002) 207.
[13] T. Ma, K. Inoue, K. Yao, H. Noma, T. Shuji, E. Abe, J. Yu, X. Wang, B. Zhang, J. Electroanal. Chem. 537 (2002) 31.
[14] J.-J. Lagref, Md.K. Nazeeruddin, M. Grätzel, Synth. Met. 138 (2003) 333.
[15] U. Bach, D. Lupo, M. Grätzel, Nature 395 (1998) 583.
[16] B. O'Regan, F. Lenzmann, R. Muis, J. Wienke, Chem. Mater. 14 (2002) 5023.
[17] T. Kitamura, M. Maitani, S. Yanagida, Chem. Lett. (2001) 1054.
[18] C. Longo, A.F. Nogueira, M.A. De Paoli, J. Phys. Chem. B 106 (2002) 5925.
[19] Y.J. Kim, J.H. Kim, M.-S. Kang, M.J. Lee, J. Won, J.C. Lee, Y.S. Kang, Adv. Mater. 16 (2004) 1753.
[20] N. Papageorgiou, W.F. Maier, M. Grätzel, J. Electrochem. Soc. 144 (1997) 876.
[21] A. Hauch, A. Georg, Electrochim. Acta 46 (2001) 3457.
[22] K. Suzuki, M. Yamaguchi, M. Kumagai, S. Yanagida, Chem. Lett. 32 (2003) 28.
[23] Y. Saito, T. Kitamura, Y. Wada, S. Yanagida, Chem. Lett. 31 (2002) 1060.
[24] Y. Saito, W. Kubo, T. Kitamura, Y. Wada, S. Yanagida, J. Photochem. Photobiol. A: Chem. 164 (2005) 153.
[25] S.-S. Kim, K.-W. Park, J.-H. Yum, Y.-Y. Sung, Sol. Energy Mater. Sol. Cells 90 (2006) 283.
[26] X. Fang, T. Ma, G. Guan, M. Akiyama, E. Abe, J. Photochem. Photobiol. A: Chem. 164 (2004) 179.
[27] X. Fang, T. Ma, G. Guan, M. Akiyama, T. Kida, E. Abe, J. Electroanal. Chem. 570 (2004) 257.
[28] K. Imoto, K. Takahashi, T. Yamaguchi, T. Komura, J. Nakamura, K. Murata, Sol. Energy Mater. Sol. Cells 79 (2003) 459.
[29] K.-W. Park, K.-S. Ahn, J.-H. Choi, Y.-C. Nah, Y.-M. Kim, Y.-E. Sung, Appl. Phys. Lett. 81 (2002) 907.